Colloid Polym Sci (2007) 285:1645–1653
DOI 10.1007/s00396-007-1736-3

ORIGINAL CONTRIBUTION

Growth of silica nanoparticles in methylmethacrylate-based water-in-oil microemulsions

S. Scholz · H. Althues · S. Kaskel

Received: 9 February 2007 / Revised: 9 May 2007 / Accepted: 28 June 2007 / Published online: 18 August 2007

Abstract The mechanism of silica particle formation in monomer microemulsions is studied using dynamic light scattering (DLS), atomic force microscopy, small-angle X-ray scattering (SAXS), and conductivity measurements. The hydrolysis of tetraethylorthosilicate (TEOS) in methylmethacrylate (MMA) microemulsions (MMA = methylmethacrylate) is compared with the formation of SiO_2 particles in heptane microemulsions. Stable microemulsions without cosurfactant were found for MMA, the nonionic surfactant Marlophen NP10, and aqueous ammonia (0.75 wt%). In the one-phase region of the ternary phase diagram, the water/surfactant ratio (R_w) could be varied from 6 to 18. The DLS and SAXS measurements show that reverse micelles form in these water-in-oil (w/o) microemulsions. The minimum water-to-surfactant molar ratio required for micelle formation was determined. Particle formation is achieved from the base-catalyzed hydrolysis of TEOS. According to atomic force microscopy measurements of particles isolated from the emulsion, the particle size can be effectively tailored in between 20 and 60 nm by varying R_w from 2–6 in heptane w/o microemulsions. For MMA-based microemulsions, the particle diameter ranges from 25 to 50 nm, but the polydispersity is higher. Tailoring of the particle size is not achieved with R_w, but adjusting the particle growth period produces particles between 10 and 70 nm.

Keywords Silica nanoparticles · Reverse microemulsions · Acrylates · Dynamic light scattering · Atomic force microscopy

S. Scholz · H. Althues · S. Kaskel (✉)
Department of Inorganic Chemistry,
Technical University of Dresden,
Mommsenstr. 6,
01069 Dresden, Germany
e-mail: Stefan.Kaskel@chemie.tu-dresden.de

Introduction

Micelles, dispersed in the oil phase of reverse microemulsions (water-in-oil microemulsions, w/o MEs) have aqueous cores, which are used as a confined space for precipitation reactions to control particle size, shape, and interparticle spacing [1–8]. Although the use of surfactants and large amounts of oil phases is limiting commercial applications, MEs have been used to a large extent for the synthesis of nanoparticles [8–15]. The main purpose of this work was to study the impact of acrylate-based oil phases in the nanoparticle formation in reverse MEs. For this reason, a single microemulsion approach was used, and the base-catalyzed hydrolysis and condensation of an alkoxide precursor [tetraethyl orthosilicate, TEOS, $Si(OEt)_4$] was carried out inside the reverse micelles [6]. The precursor diffuses into the aqueous cores of the reverse micelles, and the reaction takes place according to the following overall reaction:

$$Si(OR)_4 + 2\ H_2O \rightarrow SiO_2 + 4\ ROH$$

For the integration of inorganic particles into transparent polymers, not only particle size control is important, but also, the particles need to be separated from each other in the composite, as aggregates lead to turbidity. However, dry particles synthesized in the ME process are often difficult to redisperse in monomers, as after the formation of aggregates in the separation process (flocculation, drying etc.), agglomerates cannot be broken up any more. Consequently, it is highly desirable to avoid the necessity of particle isolation. If, however, the particles are generated in a ME in which the surrounding oil phase is itself a monomer, the isolation process is obsolete (in situ generation, ISG). Thus, replacing the heptane oil phase by monomers such as MMA or other alkenes can be used for the generation of transparent plastics after ME polymerization (MEP) [16].

Table 1 Compositions of the Marlophen NP5/heptane w/o MEs

Water-to-surfactant molar ratio, R_w	Name	*m* (NH_3, 0.75 wt%)	*m* (Marlophen NP5, g)	*m* (heptane, g)
2	E	0.45	5.5	5.0
4	F	0.90	5.5	5.1
6	G	1.35	5.5	5.0
8	H	1.81	5.5	5.0

The ISG and microemulsion polymerization (ISG-MEP process) can be seen as complementary to freeze fracture techniques, as freezing MEs reveals information about structural features of enclosed particles. However, structural changes occurring during the polymerization process (minutes to hours) will also significantly influence the secondary agglomerate structure, and thus, a direct connection between the composite structure and the ME is difficult. In this context, a better understanding of particle formation processes in monomer MEs would be helpful. Hereafter, the influence of the polymerization process on the ME stability needs to be studied. In this work, the particle formation in MMA-based MEs was studied using different techniques giving complementary information on the particle size and growth kinetics. Viscosimetry, conductivity measurements, dynamic light scattering, and small-angle X-ray scattering are used for the characterization of the MEs; atomic force microscopy is used for imaging the particles formed in the MEs. The formation of SiO_2 in MMA-based MEs will be compared to the formation in conventional heptane MEs using nonionic polyoxyethylene nonylphenyl ether surfactants (which will be abbreviated as NP*x*, where *x* is the average number of oxyethylene groups per surfactant molecule). The silica particles synthesized in w/o MEs have average sizes in the range between 10 and 70 nm. The stability and final size distribution of silica particles in the ME is affected by the amount of water and surfactant as well as the characteristics of the surfactants [17, 18].

Experimental section

Materials and sample preparation The surfactants (Nonylphenyl polyethoxylates) Marlophen NP5 (NP5) and Marlophen NP10 (NP10) were supplied by SASOL. Heptane (>99%), methylmethacrylate (99%), as well as tetraethyl orthosilicate (TEOS; 99%) were purchased from Aldrich. They were used as received. All the aqueous solutions were prepared in deionized water at 20 °C. To study the effect of the water concentration on the ME structure, the surfactant-to-water molar ratio (R_W) was modified between 2 and 8 for the heptane–NP5 system and between 10 and 18 for the MMA–NP10 system. MEs were prepared by adding the appropriate amount of water to the corresponding stock solution of NPx in heptane or MMA and stirring until the solution became transparent. Tables 1 and 3 give the compositions of the MEs used. The particle formation begins with the addition of TEOS to the transparent ME. For the heptane emulsions, 1 g TEOS was added to the MEs listed in Table 2. For the MMA emulsions, the amount of TEOS added is listed in Table 4. Transparent, opaque, or cloudy dispersions are received depending on reaction time and ME composition.

Conductivity measurements The electrical conductivity of four different compositions of MMA MEs was measured in one test series at constant temperature (20 °C) and in another test series between 5 and 35 °C using a WTW multi-lab 540 measuring probe WTW Tetracon® 325/Pt and a SevenMulti Conductivity InLab®710 conductometer from Mettler Toledo. The constant of the cell was 0.53 cm^{-1} for the WTW conductometer and 0.56 cm^{-1} for the Mettler Toledo conductometer. The measurements were carried out with alternating potential; the frequency was 50 Hz. The temperature was controlled by means of a thermostat/cryostat from MLW type U4.

Viscosimetry, determination of density, and refractive index The viscosity of the MEs was measured at 20 °C with Ubbelohde viscosimeters type 532-01-0c and type 532-13-Ic by Schott. The mean value out of four measurements is given. The determination of the density was accomplished by weighing with the help of 10-ml volumetric flasks. The refractive indices of the MEs were determined at 20 °C using an Abbé refractometer. The refractive index of pure methylmethacrylate is 1.414 (20 °C).

Table 2 Average particle height of silica nanoparticles from Marlophen NP5/heptane w/o MEs detected with atomic force microscopy

Water-to-surfactant molar ratio, R_w	Aver. particle height (nm)	Rel. SD (%)	Abs. SD (nm)	Particles counted
2	22	3	±1	20
4	40	10	±4	20
6	62	11	±6	20
8	23	3	±1	20

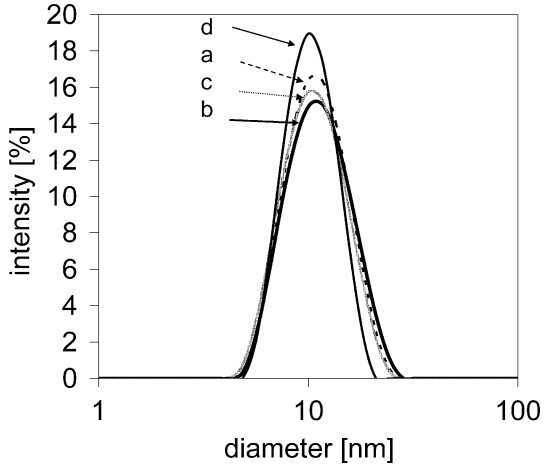

Fig. 1 Size distributions (DLS) of micelles in MEs *a* (R_w=2), *z*-average=10.2, *b* (R_w=4) z average=11.7, *c* (R_w=6) z average=11.5, and *d* (R_w=8), z average=14.9

Dynamic light-scattering measurements Dynamic light scattering (DLS) was used to estimate the apparent hydrodynamic diameter of micelles and particles in the sample solution. DLS measurements were performed with a Zetasizer Nano ZS backscattering apparatus from Malvern Instruments. The apparent hydrodynamic radius, R_h^{app} was estimated from the apparent diffusion coefficient D_m using the Stokes–Einstein equation, $R_h^{app} = k_B T/(6\pi\eta D_m)$ where T is the absolute temperature, k_B is the Boltzmann constant, and η is the viscosity of the ME resp. the viscosity of pure heptane in case of the NP5/heptane w/o MEs at a given temperature. To remove dust particles, the solutions were filtered before measurements with hydrophobic PTFE filters (0.2 μm). The scattering cell was held at 20 °C.

Atomic force microscopy Samples were prepared by spincoating one drop of the dispersion (ME after addition of TEOS) on a freshly cleaved mica substrate with a SPIN150 (SPS) at 3,000 rpm for 30 s or by using micropipettes for application of the dispersions onto the mica substrate. The coated mica substrates were washed by dipping in acetone (p. a.) to remove excess surfactant and dried with argon. The atomic force microscope used was a Dimension 3100 with Nanoscope IV SPM controller from Veeco Instruments. The tapping mode in air was applied using Veeco Nanoprobe tips, RTESP (TAP300 Metrology Probes, k=40 N/m, l=125 μm, ν=300 kHz). Atomic force microscopy (AFM) height measurements were calibrated using a standard grid (DI 10 μm pitch, 200 nm deep, 3D reference).

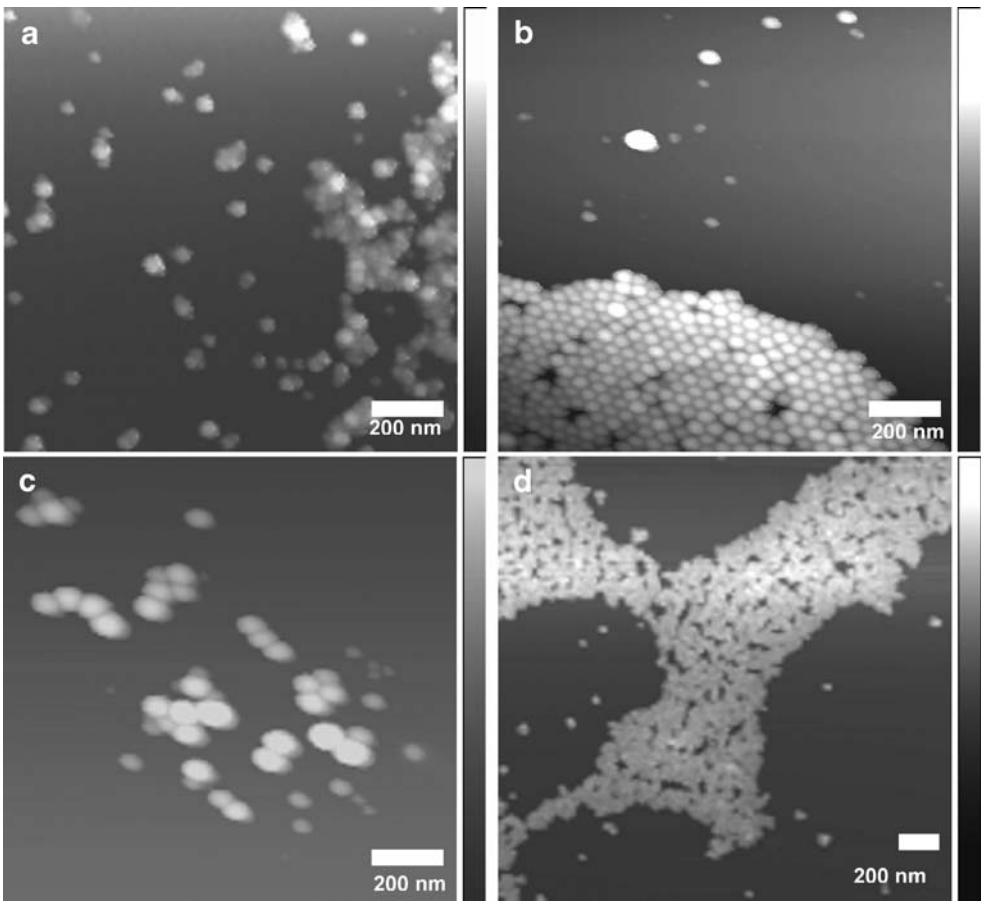

Fig. 2 AFM height images of silica particles on a mica substrate: **a** R_w=2; scan size, 5 μm; scan rate, 0.3 Hz; data scale, 100 nm; **b** R_w=4; scan size, 1.7 μm; scan rate, 0.2 Hz; data scale, 100 nm; **c** R_w=6; scan size, 5 μm; scan rate, 0.1 Hz; data scale, 150 nm; **d** R_w=8; scan size, 10 μm; scan rate, 0.5 Hz; data scale, 100 nm

Table 3 Compositions of the Marlophen NP10/methylmethacrylate w/o MEs

R_w	Name	m (NH_3, 0.75 wt%, g)	m (MMA, g)	m (Marlophen NP10, g)	Opt. prop.	κ (S/m)	n	ρ (g/cm^3)	η (cP)
6	ME RW=6	0.6	15.4	4.0	Opaque	$7.0\ 10^{-5}$	1.4301	0.9631	1.52
9	ME RW=9	1.0	15.0	4.0	Clear	$8.0\ 10^{-5}$	1.4340	0.9632	1.85
10	ME RW=10	1.2	14.8	4.0	Clear	$1.0\ 10^{-4}$	1.4270	0.9648	2.11
12	ME RW=12	1.4	14.6	4.0	Clear	$1.4\ 10^{-4}$	1.4262	0.9630	2.63
13	ME RW=13	1.5	14.5	4.0	Clear	$9.2\ 10^{-4}$	1.4315	0.9674	2.64
14	ME RW=14	1.6	14.4	4.0	Clear	$7.0\ 10^{-4}$	1.4255	0.9694	3.42
15	ME RW=15	1.7	14.3	4.0	Clear	$5.8\ 10^{-4}$	1.4254	0.9653	3.85
16	ME RW=16	1.8	14.2	4.0	Clear	$2.1\ 10^{-3}$	1.4245	0.9733	4.38
17	ME RW=17	1.9	14.1	4.0	Clear	$5.7\ 10^{-3}$	1.4244	0.9670	5.03
18	ME RW=18	2.0	14.0	4.0	Clear	$9.0\ 10^{-3}$	1.4238	0.9711	6.52

Small-angle X-ray scattering All measurements were performed with a small-angle X-ray-scattering (SAXS) device (Nanostar) from Bruker. The distance between sample and detector was 64 cm, and the q range was in between 0.02 and 0.3 Å^{-1}. The liquid samples were filled in 1- or 2-mm-thick quartz capillaries. As reference, the pure solvent was used. The graphic presentation and the fitting of the scattering curves were accomplished with the Mathcad program. The pair distance distribution functions $P(R)$ were calculated with the GNOM (Svergun) program. For the calculation of the micelle diameter D, a spherical micelle shape was assumed. The diameter was estimated from the Guinier radius $D = 2R_g(5/3)^{0.5}$.

Results and discussion

The micelle size depends on the ME composition, the temperature, and the surfactant type used. Silica nanoparticles synthesized in nonionic w/o MEs usually have a narrow size distribution with the average value between 5 and 70 nm [19]. To understand the influence of different parameters in methylmethacrylate-based reverse MEs, the results are compared with a well-known model system using heptane as the oil phase.

Dynamic light scattering, NP5/heptane w/o MEs For dynamic light scattering measurements, MEs with increasing R_w from 2 to 8 for the Marlophen NP5/heptane w/o MEs were prepared (Table 1). Figure 1 gives size distributions of micelles in MEs with increasing R_w values. The average micelle size increases from R_w=2 (10 nm) to R_w=8 (15 nm). The two micelle size distributions in between (R_w=4 and R_w=6) are almost identical. The polydispersity indices (PDIs) for the MEs are between 0.08 and 0.22, indicating monomodal distributions for small R_w and significant broadening with increasing R_w.

Atomic force microscopy, NP5/heptane w/o MEs The particle height was measured after particle formation inside the ME and subsequent deposition onto a freshly cleaved mica substrate using micropipettes and careful washing with acetone. Although a small amount of residual surfactant present on the substrate may affect the height measurements, the error is below the absolute standard deviations observed. Figure 2 shows height images of these silica particles on a mica substrate. The R_w of the corresponding MEs was 2 (Fig. 2a), 4 (Fig. 2b), 6 (Fig. 2c), and 8 (Fig. 2d; Table 1). Nano-sized particles are detected separated from each other or in the form of monolayers and with narrow size distribution. The particle size increases in a monotonic fashion from 22 nm (R_w=2) to 62 nm (R_w=6), but for the highest R_w=8, a sudden decrease is observed (Table 2). Especially for high R_w values close to the phase boundary,

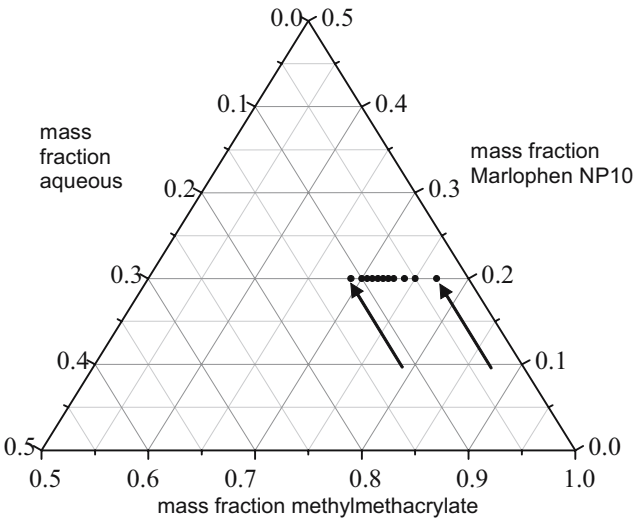

Fig. 3 Oil-rich region of the ternary phase diagram for Marlophen NP10/methylmethacrylate w/o MEs. The *solid circles* mark the compositions for MEs with R_w=9–18. The *arrows* mark the phase boundary

small changes in the ME composition caused by the addition of the precursor and subsequent release of side products (ethanol) from the hydrolysis reaction may significantly alter the ME structure, and thus, may be responsible for the irregularity observed.

Dynamic light scattering, NP10/MMA w/o MEs For dynamic light scattering measurements, MEs with increasing R_w from 10 to 18 were prepared (Table 3). The mass fraction of surfactant was kept constant. In Fig. 3, the composition of the methylmethacrylate/Marlophen NP10 w/o MEs is shown. The arrows mark the phase boundaries. Thus, a direct comparison to the heptane oil phase is restricted due to the higher HLB needed for the solubilization of significant amounts of water; a second limitation is the phase boundary. The size distribution of micelles was measured at 20 °C. Figure 4 gives size distributions of micelles in MEs with increasing R_w values. The *z*-average varies from 5 to 20 nm. For the MEs with R_w=10, 12, and 18, the polydispersity indices were between 0.29 and 0.52. The latter indicates very broad distributions in micelle size. For the MEs in between R_w=14 and 17, the polydispersity indices are lower. They range from 0.11 to 0.22. For this reason, the MEs with medium R_w values were chosen for further investigations (conductivity and particle growth measurements).

Conductivity measurements, NP10/MMA w/o MEs The measurement of electrical conductivity can be applied to study the connectivity of aqueous components in nonionic w/o MEs [19]. In contrast to the heptane-based model system, it was a problem to find a single-phase region with variable amount of the aqueous phase but without using large quantities of surfactant. After finding such compositions, it seemed interesting to check if the respective MEs are located far or close to a phase boundary. The identification of the cloud point is sometimes hard to determine by the naked eye. Using conductivity measurements, the cloud points of the MEs were clearly identified. It is well known that the conductivity of water-in-oil MEs changes with the water concentration. At higher water content, the conductivity is comparable to that of electrolyte solutions. However, at lower water concentration, the drop conductivity sharply decreases by 3–4 orders of magnitude because of the percolation threshold.

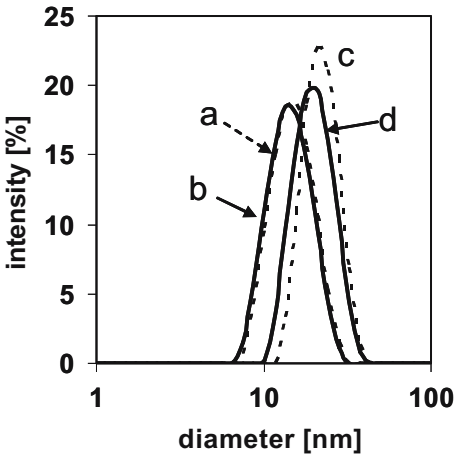

Fig. 4 Size distributions (DLS) of micelles in MEs with R_W=14 (*z*-average=12.7), R_W=15 (*z* average=12.3), R_W=16 (*z* average=20.2), and R_W=17 (*z* average=18.1) with increasing R_w from *a* to *d*

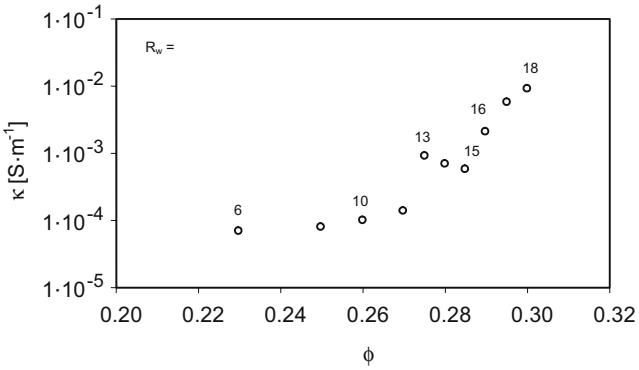

Fig. 5 Variation of the specific conductivity, κ, with increasing droplet mass fraction of w/o MEs of Marlophen NP10 dissolved in methylmethacrylate (increasing R_w)

Percolation can be also induced at constant water volume fraction by increasing the temperature. In both cases, the electrical conductivity measurements are routinely used for detecting the percolation threshold. Below the percolation threshold, the conductivity decreases with decreasing volume fraction of water, but is an order of magnitude higher than the solvent conductivity. This higher conductivity of w/o MEs has been explained by the charge fluctuation model (CFM). This model considers that the charged droplets are formed by a spontaneous number of fluctuations of the ions in the droplets. The magnitude of these fluctuations is related to the Coulomb energy required to charge up the droplet. According to this model, the conductivity κ of a dilute ME can be expressed by

$$\kappa = \varepsilon_0 \varepsilon k \Phi / 2\pi\eta r^3$$

where ε_0 is the dielectric permittivity of the vacuum, ε is the dielectric constant of the solvent, r is the droplet radius, and Φ is the mass fraction of drops: $\Phi=(m_{\text{ammonia}} + m_{\text{Marlophen NP10}})/(m_{\text{ammonia}} + m_{\text{Marlophen NP10}} + m_{\text{MMA}})$ [20, 21].

Figure 5 presents the individual conductivity values for w/o MEs composed of aqueous ammonia, methylmethacrylate, and Marlophen NP10 with Φ between 0.23 and 0.3 (R_w between 6 and 18) at a constant temperature of 20 °C. The conductivity is as small as for w/o MEs expected. Nevertheless, it is recognizable that with rising

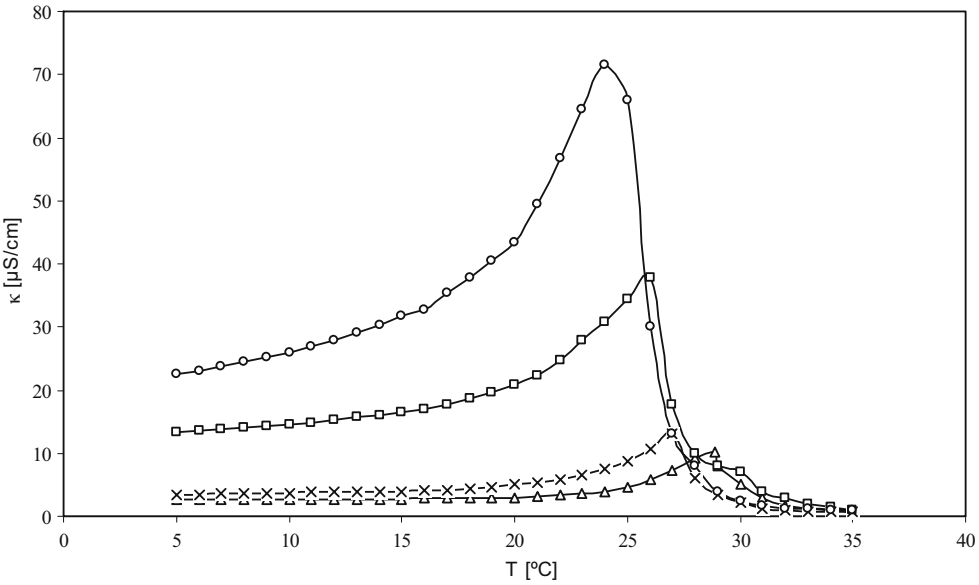

Fig. 6 Temperature dependence of the electrical conductivity of Marlophen NP10/methylmethacrylate w/o MEs containing different droplet mass fractions: *circles* Φ=0.295 (R_w=17); *squares* Φ=0.290 (R_w=16); *crosses* Φ=0.285 (R_w=15); *triangles* Φ=0.280 (R_w=14)

ammonia portion, i.e., with rising volume fraction of water, the conductivity increases continuously. As can be seen in the figure, the specific conductivity is approximately constant until Φ=0.27 (R_w=12). At Φ>0.27 (R_w>12), the conductivity sharply increases. The regime of constant specific conductivity can be identified with dilute water-in-oil MEs. A reason for the weak R_w dependence at this region are Coulombic as well as short-range interactions between droplets [21, 10]. The sharp increase of specific conductivity is, on the other hand, not high enough to show evidence of percolation. The CFM from Eicke et al. does not account for nonspherical droplet shape and polydispersity, and the percolation cannot be described.

The conductivity of MEs formed at constant R_w at different temperatures was also determined. To identify the high-temperature limit for the microemulsion polymerization, temperature-dependent conductivity measurements were carried out. Four MEs composed of ammonia, methylmethacrylate, and Marlophen NP10 with different R_w above R_w=12 were selected, whereas the ammonia concentration remains constant. Figure 6 presents these conductivity values. From the figure, percolation was observed for temperatures between 24 °C for the ME with highest R_w= 17 and 29 °C for the ME with smallest R_w=14. The conductivity maxima correspond to the cloud point (Krafft point). In the case of alkylpolyethylenoxides, the cloud point correlates with the phase-inversion-temperature, but they are not equivalent. Shortly after the cloud point is reached, strong streak formation is noticeable. Above this characteristic temperature (Krafft point), phase separation occurs. Conductivity results indicate that the droplet mass fraction 0.29 (R_w=16) seems to be a critical value because of the sharp increase above this droplet mass fraction. This could be due to structural changes of the droplets.

Atomic force microscopy, NP10/MMA w/o MEs For the estimation of the particle height, particles were studied from TEOS hydrolysis in four different MEs. The parameters and compositions are listed in Table 4. After 20 h of stirring at constant temperature (20 °C), the dispersions were spread on a freshly cleaved mica substrate using a spin coater. To remove the surfactant sticking on the silica surface, the

Table 4 Average particle height of silica nanoparticles from Marlophen NP10/methylmethacrylate w/o MEs detected with atomic force microscopy

Water-to-surfactant molar ratio, R_w	Volume TEOS (ml)	Aver. particle height (20 h reaction time, nm)	Rel. SD (%)	Abs. SD (nm)	Particles counted
14	0.84	28	15	±4	54
15	0.90	27	18	±5	20
16	0.95	27	33	±9	19
17	1.00	50	20	±10	150

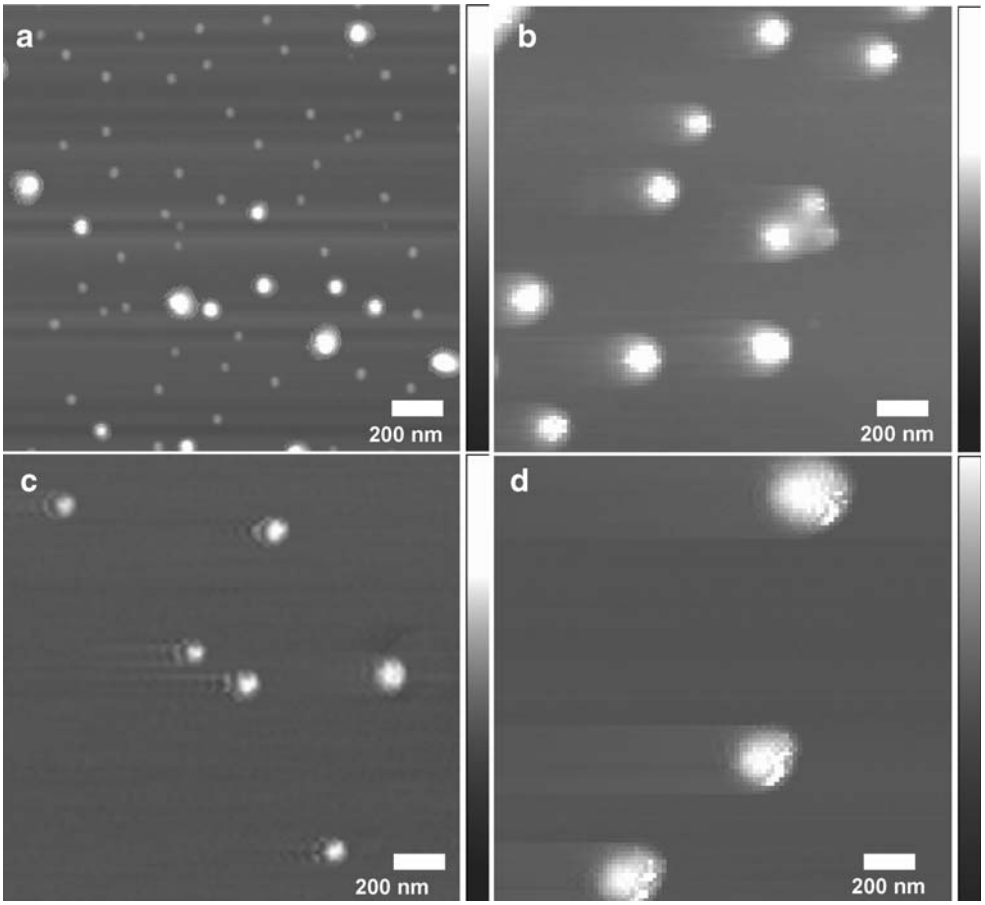

Fig. 7 AFM height images of silica particles on a mica substrate: **a** R_w=14; scan size, 2.1 μm; scan rate, 0.5 Hz; data scale, 50 nm; **b** R_w=15; scan size, 3.7 μm; scan rate, 1.0 Hz; data scale, 195 nm; **c** R_w=16; scan size, 5.2 μm; scan rate, 1.0 Hz; data scale, 60 nm; **d** R_w=17; scan size, 10 μm; scan rate, 1.0 Hz; data scale, 110 nm

mica substrate was dipped into acetone. Nevertheless, a part of it remains on the surface so that it was difficult to get useful AFM height images because of interactions of the tip and the surfactant on the particles. Figure 7 shows the height images of these silica particles on a mica substrate. The R_w of the corresponding MEs was 14 (Fig. 7a), 15 (Fig. 7b), 16 (Fig. 7c), and 17 (Fig. 7d; Table 4). Nano-sized particles are detected separated from each other. For the first three samples, there is no difference in particle height, but the height profiles of the particles of the last sample are higher. With increasing R_w, the standard deviation is also increasing. The particles are between 27 nm (R_w=15) and 50 nm (R_w=17) in height. Table 4 gives information about the particle height. Thus, in comparison to the heptane microemulsions, tailoring of the silica particle size inside the MMA MEs is more difficult. One reason is the narrow range of R_w values accessible in MMA-based MEs. As the R_w value increase from 14 to 17 is much lower compared to the heptane emulsion (R_w=2–8), the differences in particle diameter are not as pronounced. A key difference between the two systems is the higher polydispersity of the droplets in the MMA ME, resulting in a higher polydispersity of the silica particles as well.

Small-angle X-ray scattering, NP10/MMA w/o MEs The results of the SAXS experiments are listed in Table 5. The micelle diameters of the three analyzed MEs are independent from the R_w value and close to 15 nm. In contrast to the model ME system in which heptane forms the oil phase, a significant increase of the micelle size with increasing R_w was not observed. In Fig. 8a, the angular dependence of scattered X-ray intensity from the three MEs (R_W=9, 13, and 17) is illustrated. The corresponding pair distance distributions are shown in Fig. 8b. GNOM and Guinier analysis are consistent, and the size curves are symmetric. The SAXS results are not in good agreement with the DLS data in which at least some increase of the hydrodynamic diameter

Table 5 Results of the SAXS size analysis

Water-to-surfactant molar ratio, R_w	*D* (Guinier, nm)	D (GNOM, nm)
9	16.4	17.3
13	15.0	16.2
17	15.0	16.2

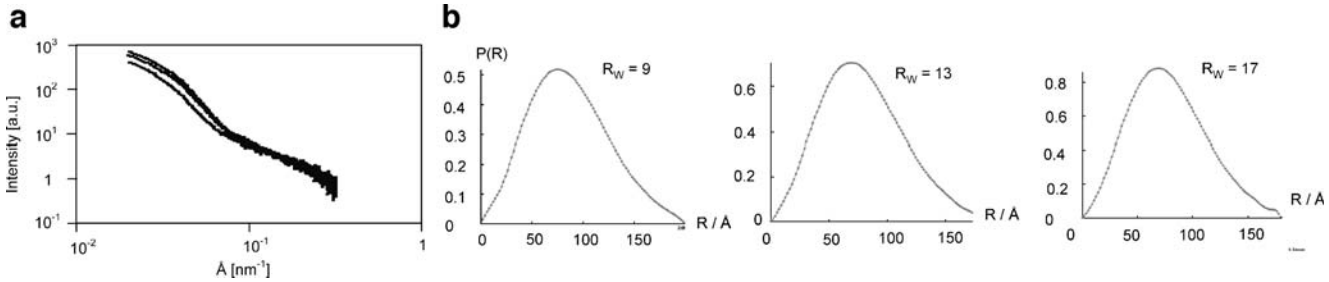

Fig. 8 **a** Angular dependence of scattered X-ray intensity (SAXS) from three samples of Marlophen NP10/methylmethacrylate w/o MEs (R_W=9, 13, and 17). **b** Pair distance distributions calculated from the SAXS data of three Marlophen NP10/methylmethacrylate w/o MEs (R_W=9, 13, and 17)

from R_W=14 (z average=12.7) to R_W=17 (z average=18.1) was observed. However, for the MMA MEs also, the viscosity significantly increases, and thus, the application of the Stokes–Einstein equation may be limited due to intermicellar interactions. The limited variability of the micelle diameter indicated from the SAXS measurements is in good agreement with the limited adjustability of the silica particle diameter in MMA MEs as discussed in the previous section. However, the particle size obtained from the single ME technique not only depends on composition but also on the growth kinetics.

Growth of silica particles The kinetics of silica particle growth in four MEs with the R_w values 14, 15, 16, and 17

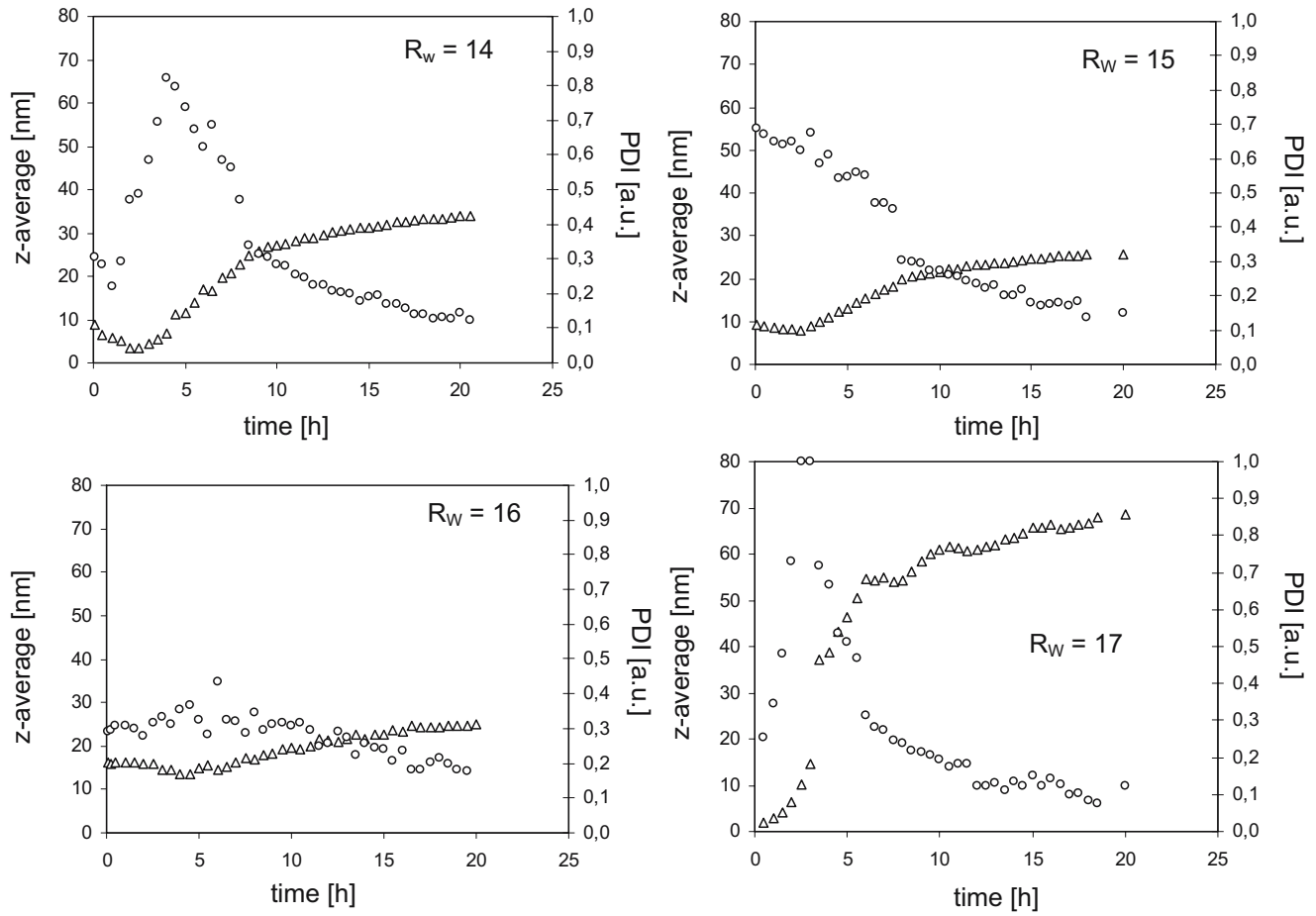

Fig. 9 Time dependence of the silica-particle growth for four different MEs with R_w values 14, 15, 16, and 17: *circles*, polydispersity index (PDI) of the size distributions; *triangles*, z-averages

Table 6 Time dependence of silica particle growth, average sizes, and polydispersity investigated by DLS

Water-to-surfactant molar ratio, R_w	Reaction time (h)	*z*-average (nm)	PDI	Reaction time (h)	*z*-average (nm)	PDI
14	4	7	0.82	20	34	0.14
15	3	9	0.67	20	26	0.15
16	6	14	0.44	20	25	0.18
17	3	15	1	20	69	0.12

were investigated by dynamic light scattering and atomic force microscopy. The average size (*z*-average) and the polydispersity (PDI) of these size distributions are shown in Fig. 9. In all four cases, a plateau is reached after 10 h. At the beginning of the curves (between 3 and 4.5 h), a slight decrease of *z*-average is noticeable. At this point, the particle growth starts. The particle sizes are between 7 and 15 nm as can be seen from Table 6. At this position, the polydispersity indices are high in some cases, but after some reaction time, the polydispersity indices decrease. During the initial reaction period, the measurements of the average particle size show the formation of quite small but non-uniform particles and a quick growth. With proceeding duration, the particle sizes increase. After 10 h of reaction time, the particle growth slows down to approximately 0.5–1 nm/h, and after 20 h of reaction time, nearly uniform particles with average particle sizes between 25 and 69 nm are obtained. The polydispersity indices range from 0.12 to 0.18. The average particle size after 20 h of reaction time estimated by DLS correlates well with the particle sizes determined with AFM (Fig. 7; Table 4). Thus, tailoring the particle size in MMA-based MEs is probably more efficiently carried out by adjusting the duration of the reaction to the particle size needed.

Conclusion

In the used model system consisting of heptane/Marlophen NP5/ammonia, it is possible to a certain extent to control the micelle size (determined with DLS) as well as the particle size of the silica nanoparticles (determined with AFM) by adjusting the water-to-surfactant molar ratio (R_w).

To apply the same concept for a polymerizable system like MMA/Marlophen NP10/ammonia, the MEs were investigated by conductivity measurements, DLS, and SAXS. Thereby, it was found that above a certain water content, reverse micelles are existent, but the micelle size is not as simple to control as in the model system. One reason for this non-transferability could be the different polarities of the oil phases used: Heptane is an apolar solvent and not miscible with the aqueous phase. Methylmethacrylate, in contrast, is a partially water-soluble monomer. Thus, MMA in the aqueous phase has a strong influence on the formation of micelles. Furthermore, the R_w alone seems not to be sufficient to control the micelle size. Due to these difficulties, in the MMA/Marlophen NP10/ammonia MEs, the particle size cannot be controlled with the composition, but only with the duration of the reaction.

References

1. Grasset F, Marchand R, Marie AM, Fauchadour, D, Fajardie FJ (2006) Colloid Interface Sci 299:726
2. Boutonnet M, Kizling J, Touroude R, Maire G, Stenius P (1991) Catal Letters 9:347
3. Boutonnet Kizling M, Bigey C, Touroude R (1996) Appl Catal A 135:L13
4. Boutonnet Kizling M, Regali F (1998) Stud Surf Sci Catal 118:495
5. Fang JY, Wang J, Ng SC, Chew CH, Gan LM (1997) Nanostruct Mater 8:499
6. Althues H, Kaskel S (2002) Langmuir 18:7428
7. Texter J (2001) Reactions and synthesis in surfactant systems. Marcel Dekker, New York
8. Kumar P, Mittal KL (1999) Handbook of microemulsion science and technology. Marcel Dekker, New York
9. Pillai V, Shah DOJ (1996) Magn Magn Mater 163:243
10. Lopez Perez JA, Lopez Quintela MA, Mira J, Rivas J, Charles SWJ (1997) Phys Chem B 101:8045
11. Lopez-Quintela MA, Quiben-Solla J, Rivas J (1997) Surf Sci Series 66:247
12. Mira J, Lopez-Perez JA, Lopez-Quintela MA, Rivas J (1997) Mater Sci Forum 235–238:297
13. Tojo C, Blanco MC, Lopez-Quintela MA (1998) Synthesis of nanoparticles in microemulsions: a comparisons study between experimental and simulation results. In Proceedings of the International Workshop on Non-Crystalline Solids, Santiago de Compostela, vol 5, World Scientific, Singapore, pp 451–456
14. Li Y, Park CW (1999) Langmuir 15:952
15. Lopez-Quintela MA, Rivas J, Blanco MC, Tojo C (2003) Nanoscale Mater 135
16. Palkovits R, Althues H, Rumplecker A, Tesche B, Dreier A, Holle U, Fink G, Cheng CH, Shantz DF, Kaskel S (2005) Langmuir 21:6048
17. Chang C-L, Fogler HS (1996) AIChE Journal 42:3153
18. Osseo-Asare K (2000) Surf Sci Series 92:147
19. Chang C-L, Fogler HS (1997) Langmuir 13:3295
20. Eicke HF, Borkovec M, Das-Gupta BJ (1989) Phys Chem 93:314
21. Velazquez MM, Valero M, Ortega FJ (2001) Phys Chem B 105:10163